Geomechanics and Engineering, *Vol. 14, No. 2 (2018) 187-193*
DOI: https://doi.org/10.12989/gae.2018.14.2.187

Influence of fracture characters on flow distribution under different Reynold numbers

Jing Wang[1a], Shu-Cai Li[*1],Li-Ping Li[1,2b] and Cheng-Lu Gao[1c]

[1]Geotechnical and Structural Engineering Research Center, Shandong University, Jinan 250061, Shandong, China
[2]State Key Lab of Subtropical Building Science, South China University Of Technology, Guangzhou 510005, Guangdong, China

(Received April 19, 2017, Revised July 9, 2017, Accepted July 11, 2017)

Abstract. Water inrush through the destruction of water resisting rock mass structure was divided into direct water inrush, key block water inrush and splitting water inrush. In the direct water inrush, the Reynolds numbers has a significant effect on the distribution of the water flow and vortex occurred in the large Reynolds numbers. The permeability coefficient of the fracture is much larger than the rock, and the difference is between 104 and 107 times. The traditional theory and methods are not considering the effect of inertia force. In the position of the cross fracture, the distribution of water flow can only be linearly distributed according to the fracture opening degree. With the increase of Reynolds number, the relationship between water flow distribution and fracture opening is studied by Semtex.

Keywords: water inrush; Reynolds numbers; permeability coefficient; cross fracture; the distribution of water flow

1. Introduction

In the numerical simulation study of water inrush from natural channel exposing, the evolution process of water inrush was investigated by embedding the evolution equation of water flow such as the cubic law, Poiseuille equation etc. into the commercial software. Mourzenko (1995) estimated the fracture width by inscribed cylinder diameter and the cubic law was modified. He (2010) studied on the single fracture's seepage characteristics in different joint roughness coefficients. In experiment study, a series of laboratory experiments were conducted to determine the magnitude of laminar flow interference effects at fractures by Wilson(1976). Kosakowski and Berkowitz (1999) used numerical methods to examine the variability of flow patterns in representative fracture intersection geometries (1<Reynolds numbers<100). Johnson (2006) studied fluid flow and mixed in rough-walled fracture intersections using the numerical methods. The flow field in T-jets mixers was studied experimentally for different geometrical parameters using Planar Laser Induced Fluorescence (PLIF) (Sultan *et al.* 2012).

2. Fracture characteristics and influence on seepage

There are lots of fractures in the rock mass. The permeability coefficient of fractured rock is much larger than intact rock (Zhou 2015). Its permeability coefficient is 10^4-10^7 times of the intact rock. Therefore, fractures are the main water flow channel. Based on previous research, six basic characteristics of rock fractures are analyzed as Table 1.

3. Water inrush through the destruction of water resisting rock mass structure

Water inrush through the destruction of water resisting rock mass structure (Fig. 1) include: (1) Natural channel revealed and then water inrush occurred directly. (2) Water inrush induced by local block instability. (3) Water inrush caused by local rock mass splitting instability.

(1) Natural channel revealed and then water inrush occurred directly

Because in the process of excavation, water inrush channels are directly exposed. Water inrush occurred from revealed channels

(2) Water inrush induced by local block instability

In the hard karst strata with high pressure and rich water, the surrounding rock is cut by joints and fissures into various types of spatial mosaic blocks. These blocks were in a state of natural balance before the excavation of the tunnel. After the tunnel excavation, the stability of key block lost for the release of stress and high water pressure which lead to other blocks deformation and collapse. At last, the water bearing structure connected and water inrush happened. In the formation of fault fracture zone, soft interlayer joints and strata cut by joints and fissures, the occurrence of this situation should be paid more attention.

(3) Water inrush caused by local rock mass splitting instability

∗Corresponding author, Professor
E-mail: lishucai@sdu.edu.cn
[a]Ph.D.
E-mail: wjingsdu@163.com
[b]Professor
E-mail: yuliyangfan@163.com
[c]Student
E-mail: chenglugao@163.com

http://www.techno-press.org/?journal=gae&subpage=7
ISSN: 2005-307X (Print), 2092-6219 (Online)

Table 1 Analysis of six basic characteristic of rock fractures

Type	Basic characteristic
Occurrence	Fracture occurrence is an important index to study the permeability and mechanical anisotropy of fractured rock mass. The occurrence of fractures is mainly affected by geological structure with group orientation distribution. It mainly includes three elements: direction, dip and dip angle respectively. The dip and dip angle of structure planes generally obey normal distribution or lognormal distribution. Each group of preferred structure planes has approximately the same fracture occurrence. For representing orientation of geological planar surfaces, the method of stereographic equal-area projection is frequently employed, as it accurately shows the spatial distribution of data. Basic concepts on great-circle plots and π-pole plots to represent planes can be found in any standard text on structural geology (Singhal, BBS and Gupta, RP, 2010).
Scale	The shape of fracture, the scale of fracture surface, the geometry of three-dimensional space. Statistical aspects on the bearing of fracture shape on area estimation are discussed by a few workers (Singhal, BBS and Gupta, RP, 2010).
Aperture	The aperture (width of fracture) is mainly generated by rock under the action of tensile stress or shear rupture expansion. Its size is usually closely related to the scale and mechanical cause. The larger scale of the permeability structure, the wider aperture. The width of fracture is mainly composed of average fracture width, mechanical fracture and equivalent hydraulic fracture width. Fracture aperture can be measured by various methods which include feeler gauge, fluorescent dyes, impression packer, tracer test, hydraulic test etc. Readers may refer to Indraratna and Ranjith (2001) for details of various methods used for measurement of fracture aperture.
Spacing and density	It is the index of the development degree of fracture surface in rock mass. The density is an important index that affects the strength and permeability of fractured rock mass. When the density is less than a critical value, the seepage cannot happen. The value is the critical density of seepage in fractured rock mass. Fracture separation (f_s) is related to lithology and thickness of the bed (b), and is given as (Nelson 2001) $$f_s = Y \cdot b \quad (1)$$ where Y is a constant related to lithology.
Fracture morphology	It mainly includes the roughness of the surface, the contact ratio of the area, the degree of filling and cementation respectively. The roughness refers to the roughness of the structure's side wall which has an important influence on shear strength and permeability of rock mass. It also has an important influence on the mechanical properties and hydraulic characteristics of fractured surface.
Connectivity and correlation	The connectivity of fracture network is the connectivity of a single structure plane or structure planes in same direction. The connectivity of fracture network determines the mechanical and hydraulic properties of rock mass in a certain degree. It has an important significance on the strength of structure and the shear stability along a certain direction. The correlation is the degree of correlation between the structural planes which is very important to study the permeability of rock mass. For evaluating connectivity it is necessary to study how the fractures terminate. Barton *et al.* (1987) classified fractures into three categories: abutting, crossing, and blind. The fractures of blind type do not intersect other fractures and remain unconnected.

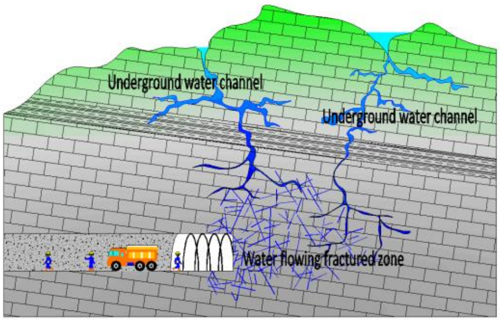

Fig. 1 Diagram of water inrush through the destruction of water resisting rock mass structure

For the deep buried tunnel, water pressure is very high. Under the action of hydrostatic pressure or dynamic water pressure, hydraulic fracturing of rock mass will happen. As the connectivity of fracture, opening degree and the permeability increased, eventually water inrush occurred (Wang 2017).

4. Flow in cross fractures

In the water inrush through Natural channel revealed, water are mainly flow in the channel. And the fractures are the main water flow channel. Although the fracture network is very complex, it is composed of fractures and intersections. There are a lot of fractures in the rock mass. The water permeability of rock mass is very intense, which is the main seepage channel of rock mass.

4.1 The Spectral/hp element method

There are several numerical methods for flow in fractures through Navier-Stokes equation such as smoothed particle hydrodynamics (Niroumand 2016, Tartakovsky 2016), lattice-Boltzmann (Wang 2017) and other numerical methods (Li 2016).

The Spectral/hp element method combined the finite element method with the accuracy of spectral method for the numerical solution of the incompressible Navier-Stokes equation. In the spectral element discretization, the computational domain was broken into a series of elements, and the velocity in each element was represented as a high-order Lagrangian interpolant through Chebyshev collocation points (Patera 1984).

Comparing with the low order finite method such as the finite element method, the finite volume method and the finite difference method, the spectral/hp element method is more efficient and accurate to obtain an approximate solution for the sufficiently problems.

The spectral element method uses a tensor product space spanned by nodal basis functions associated with Gauss–Lobatto points. In contrast, the p-version finite element method spans a space of high order polynomials by node less basis functions, chosen approximately orthogonal for numerical stability. Since not all interior basis functions need to be present, the p-version finite element method can create a space that contains all polynomials up to a given degree with fewer degrees of freedom. However, some speedup techniques possible in spectral methods due to their tensor-product character are no longer available. The name p-version means that accuracy was increased by increasing the order of the approximating polynomials (thus, p) rather than decreasing the mesh size, h.

4.1.1 Dimensionless of the NS equations

Assuming the fluid to be Newtonian and the flow incompressible, the relevant equations of motion for the primitive variables (velocities, pressure) are the incompressible NS equations.

$$\rho_0\left(\frac{\partial u}{\partial t} + u \cdot \nabla u\right) = -\nabla p + \mu \nabla^2 u \quad (2)$$

The governing equations is written in a Lagrangian form. The motion equations are

$$\rho_1 \frac{\partial^2 X}{\partial t^2} = \frac{\partial}{\partial s}\left(T \frac{\partial X}{\partial s}\right) - \frac{\partial^2}{\partial s^2}\left(\gamma \frac{\partial^2 X}{\partial s^2}\right) + \rho_1 g \tag{3}$$

The characteristic scales were applied to the dimensionless such as Dimensionless length and velocity with magnitude 1.

The non-dimensional variables are denoted by a superscript *

Length scales, the L is the characteristic length

$$x^* = \frac{x}{L}, y^* = \frac{y}{L}, z^* = \frac{z}{L}, \nabla^* = L\nabla, {\nabla^*}^2 = L^2\nabla^2 \tag{4}$$

Time scales

$$t^* = \frac{tU}{L} \tag{5}$$

Velocity U is the characteristic velocity

$$u^* = \frac{u}{U} \tag{6}$$

Pressure

$$P^* = \frac{P}{\rho U^2} \tag{7}$$

Reynolds number

$$Re^* = \frac{\rho U L}{\mu} \tag{8}$$

For convenience, in the following, the dimensionless quantities are written in the same form as their dimensional counterparts.

$$\frac{\partial u^*}{\partial t} + u^* \cdot \nabla u^* = -\nabla P^* + \frac{\nabla^2 u^*}{\mathrm{Re}} \tag{9}$$

$$\frac{\partial^2 X}{\partial t^2} = \frac{\partial}{\partial s}\left(T \frac{\partial X}{\partial s}\right) - \frac{\partial^2}{\partial s^2}\left(\gamma \frac{\partial^2 X}{\partial S^2}\right) + F^* \frac{g}{g} \tag{10}$$

$$F^* = \frac{gL^*}{U^2} \tag{11}$$

4.1.2 Linearized NS equations in operator form

The fluid we study is the incompressible. So the Navier-Stokes equation is

$$\partial_t u = -u \cdot \nabla u - \nabla p + Re^{-1}\nabla^2 u \tag{12}$$

with

$$\nabla \cdot u = 0 \tag{13}$$

where p is the modified or kinematic pressure, u is the velocity vector.

The Reynolds number Re is

$$Re = \frac{UD}{\nu} \tag{14}$$

where the U is the convenient velocity, D is the length scales and v is kinematic viscosity.

The flow field is decomposed as the sum of a base flow and a perturbation.

$$(u, p) = (U, P) + (u', p') \tag{15}$$

The changed NS equation is

$$\partial_t(U + u') = -(U + u') \cdot \nabla(U + u') - \nabla(P + p') + Re^{-1}\nabla^2(U + u') \tag{16}$$

Expand

$$\partial_t(U + u') = -U \cdot \nabla U - u' \cdot \nabla U - U \cdot \nabla u' - u' \cdot \nabla u' - \nabla P - \nabla p' + Re^{-1}\nabla^2(U + u') \tag{17}$$

Then collect into equations for evolution of the base flow

$$\partial_t U = -U \cdot \nabla U - \nabla P + Re^{-1}\nabla^2 U \tag{18}$$

So the perturbation is

$$\partial_t u' = -u' \cdot \nabla U - U \cdot \nabla u' - u' \cdot \nabla u' - \nabla p' + Re^{-1}\nabla^2 u' \tag{19}$$

The interaction of perturbations can be ignored. So the govern evolution of the infinitesimal perturbations can be written as

$$\partial_t u' = -u' \cdot \nabla U - U \cdot \nabla u' - \nabla p' + Re^{-1}\nabla^2 u' \tag{20}$$

because the flow is incompressible. The pressure can be considered as a constraint field. The gradient keeps the flow divergence-free. The pressure can be obtained from the advection terms as the solutions of a Poisson equation.

$$p' \equiv \nabla^{-2}\nabla \cdot [U \cdot \nabla + (\nabla U)^T] \cdot u' \tag{21}$$

So the NS equation can be written as

$$\partial_t u' = -[I - \nabla\nabla^{-2}\nabla] \cdot [U \cdot \nabla + (\nabla U)^T] \cdot u' + Re^{-1}\nabla^2 u' \tag{22}$$

The spatial terms are now just a linear operator applied to the perturbation velocity. So the linearized NS equations in operator form is

$$\partial_t u' - L(u') = 0 \tag{23}$$

The above notation is adopted largely for compactness/convenience and does not imply that the pressure is not computed. However, it is typically only the velocity components which are considered as part of the numerical Eigen system analysis of incompressible flows.

4.2 Influence of different fracture widths on flow distribution under different Reynolds numbers

When the fluid flows through cross fractures, the width of fractures has a significant influence on the flow field. In this section, the influence of different Reynolds numbers on the flow distribution of different fracture widths was studied. When the Reynolds number is small, the influence of viscous force on the flow field is much larger than the inertia force. Fluid flow is relatively stable, laminar flow. With the increase of Reynolds number, the influence of inertia force on fluid is greater than viscous force. However, the traditional fluid calculation software can not consider the role of inertia force. In the case of large Reynolds number, the simulation results are quite different from the actual situation. Semtex is used to simulate the fluid flow in different width of fractures.

The numerical simulation is assumed to be

(1) Fluid is incompressible fluid

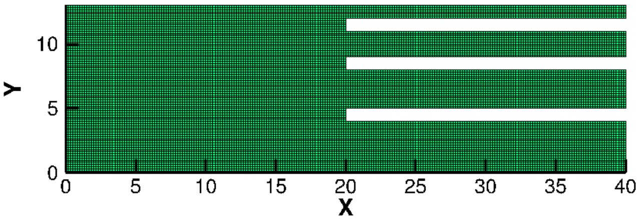

Fig. 2 The computational domain

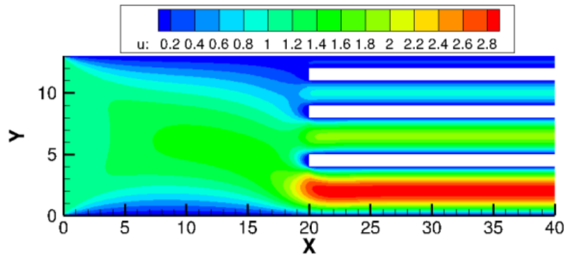

(a) Reynold numbers is 1

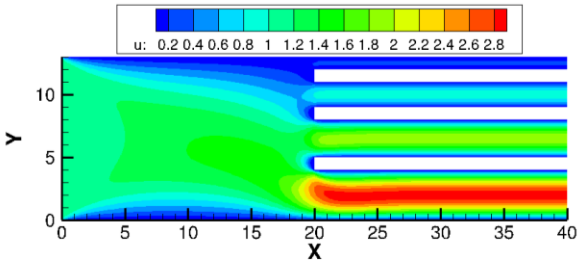

(b) Reynold numbers is 2

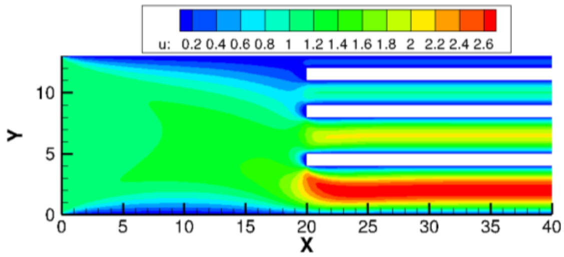

(c) Reynold numbers is 5

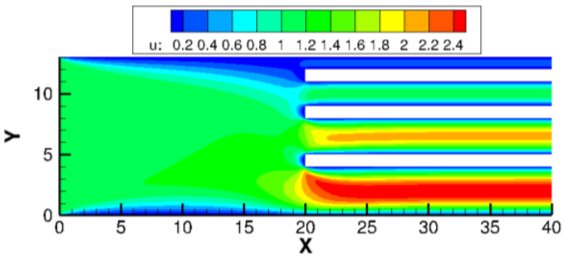

(d) Reynold numbers is 10

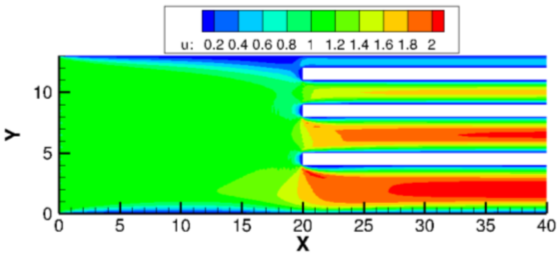

(e) Reynold numbers is 50

Fig. 3 The velocity of fluid under different Reynolds numbers

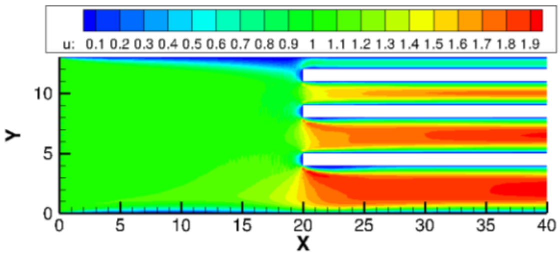

(f) Reynold numbers is 100

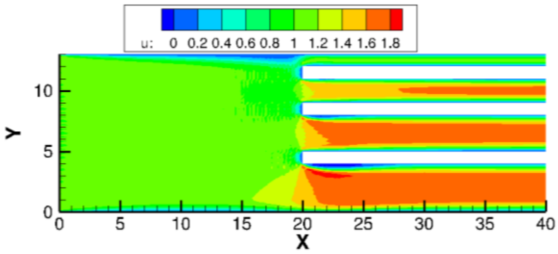

(g) Reynold numbers is 200

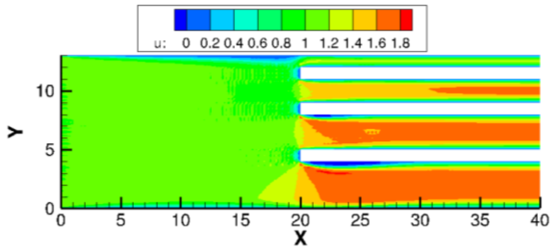

(h) Reynold numbers is 300

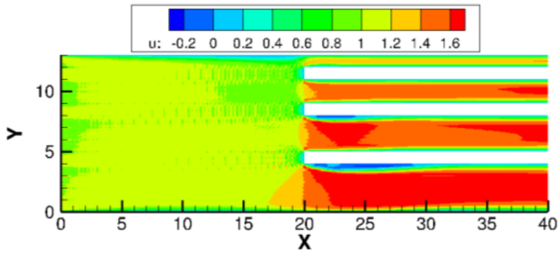

(i) Reynold numbers is 500

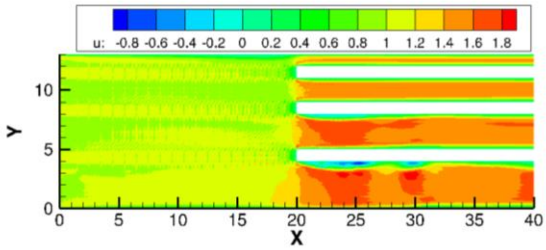

(j) Reynold numbers is 1000

Fig. 3 Continued

(2) Fluid can flow only in the fractures

(3) Through the Navier-Stokes equation to describe the flow characteristics of the fluid

The calculated parameters are as follows (dimensionless): the length and width of domain is x×y=13×40. The water inflow located at x=0 and the water outlet located at x=40. From top to bottom for outlet 1, outlet 2, outlet 3 and outlet 4. Their widths are 1, 2, 3 and 4. The Reynolds numbers were Re=1, Re=2, Re=5, Re=10, Re=50, Re=100, Re=200, Re=300, Re=500 and 1000, respectively.

The computational domain is decomposed into 1840 spectral elements and 2067 nodes in x and y directions, in each of which, piecewise continuous nodal-based polynomial expansions with polynomial order P=4 are applied. The domain is shown in Fig. 2.

The velocity of fluid under different Reynolds numbers are shown in Fig. 3.

According to the result of numerical simulation, when the Reynolds number is small, the fluid is mainly affected by the viscous force. In this range, there is no vortex appear which can be seen as laminar flow. When the Reynolds numbers increased to 300, the vortex was gradually formed in outlet three and four. The fluid vortex of water flow in the outlet four is shown in Fig. 4.

In hydrology, discharge is the volume rate of water flow which is transported through a given cross-sectional area. With the increase of Reynolds numbers, the discharge of outlet 4 is gradually decreased. The discharge of outlet 2 is almost constant. The discharge of outlet 2 and outlet 3 are gradually increased (Fig. 5).

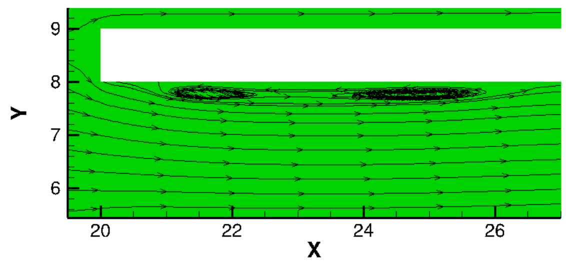

(a) Outlet three

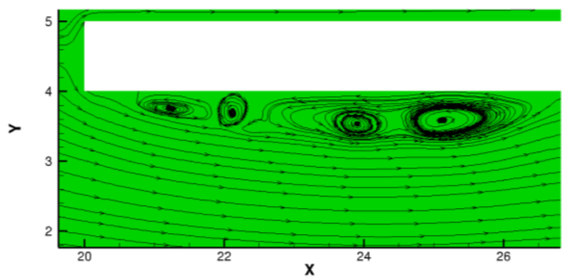

(b) Outlet four

Fig. 4 Fluid vortex of water flow in the outlet three and four (Re=1000)

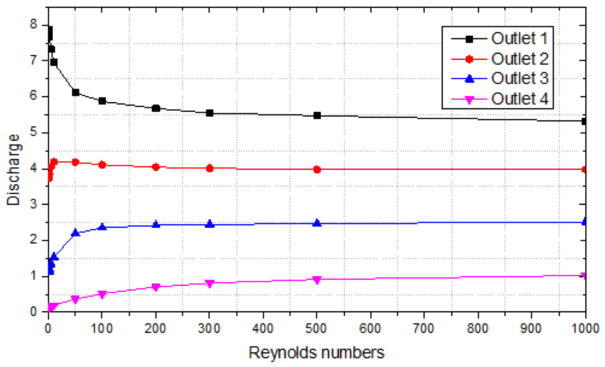

Fig. 5 The discharge of four outlets in different Reynolds numbers

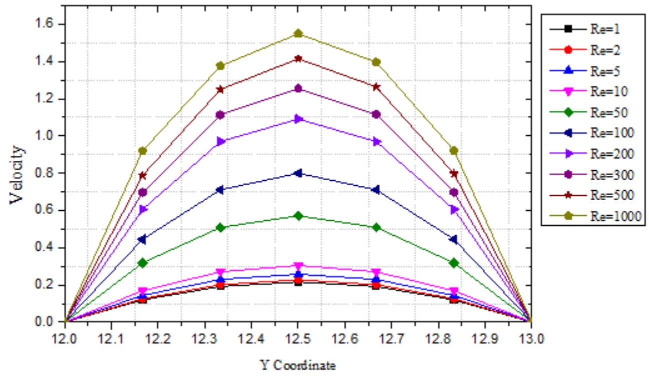

(a) Outlet one

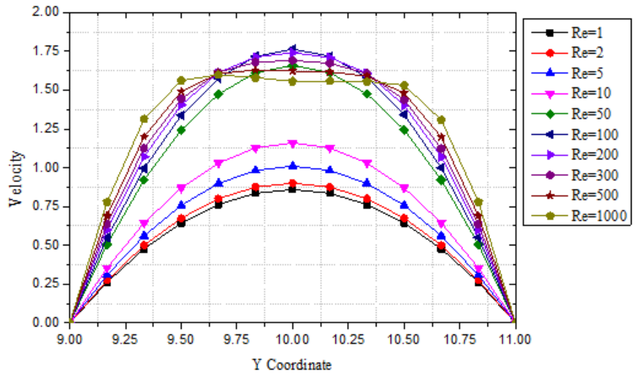

(b) Outlet two

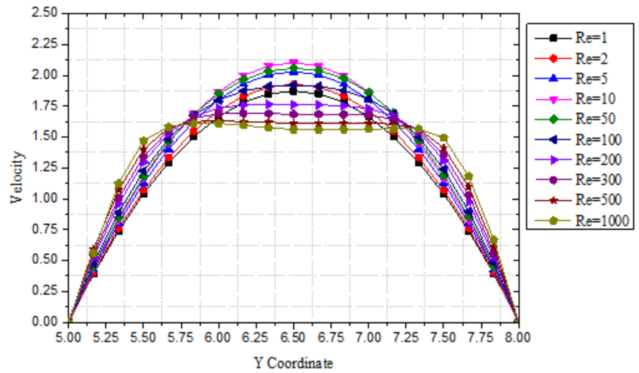

(c) Outlet three

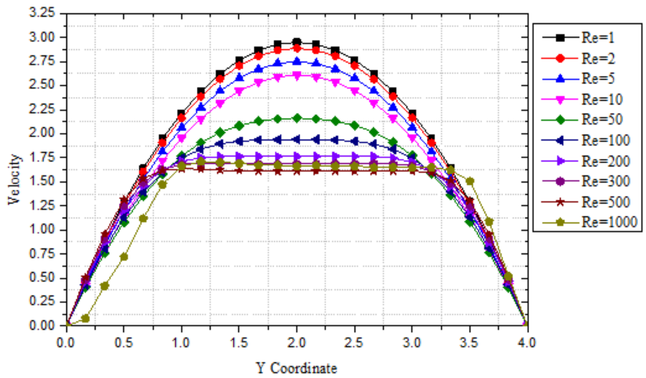

(d) Outlet four

Fig. 6 The velocity distribution in different Reynolds numbers

We can see from Fig. 6 that the velocity of outlet is larger at the middle of the fractures, smaller at both sides which presented parabola change. The velocity of outlet 1 increases gradually along with the increase of Reynolds number. The flow velocity at both sides of the outlet 2 increases gradually along with the increase of Reynolds number. The maximum flow velocity in the middle of outlet 2 is

$$V_{M1} < V_{M2} < V_{M5} < V_{M10} < V_{M1000} < V_{M500} < V_{M50} < V_{M300} < V_{M200} < V_{M100}$$

Outlet 3 and outlet 4 gradually decrease with the increase of Reynolds number.

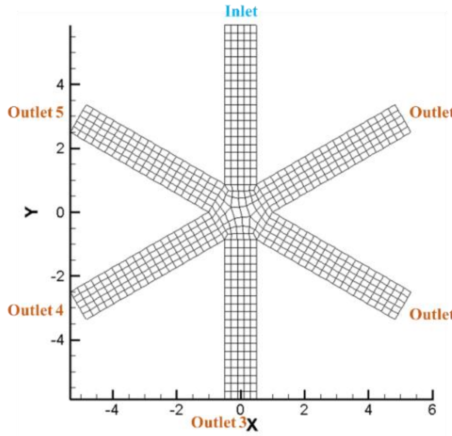

(a) Calculation model

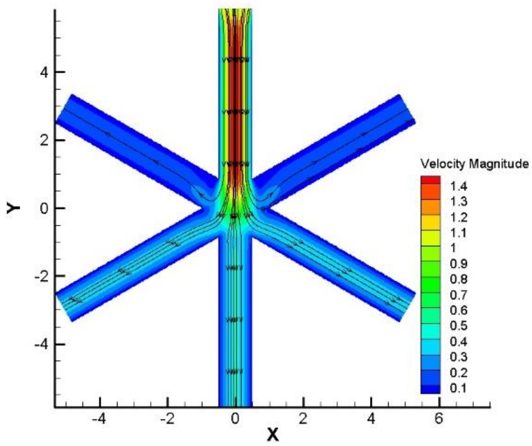

(b) Re=20

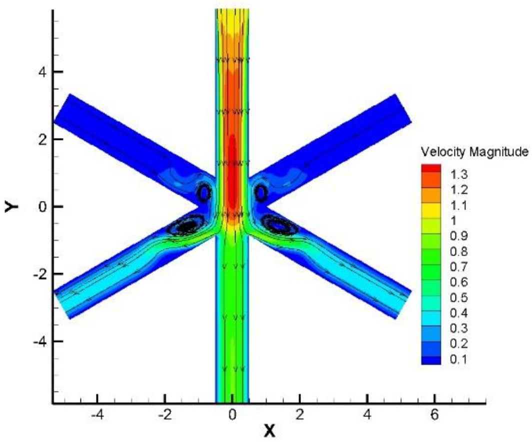

(c) Re=300

Fig. 7 Flow in the cross fractures with different Reynolds numbers

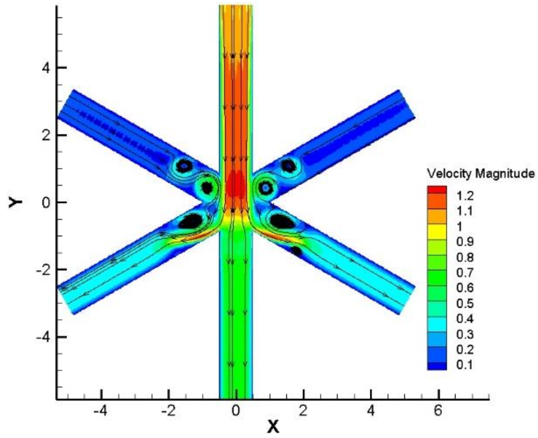

(d) Re=1000

Fig. 7 Continued

4.3 Influence of different fracture angles with different Reynolds numbers

There are lots of researches on fracture flow, but most of them concentrate on the flow with low Reynolds numbers. But the effect of Reynolds number on fracture is very large. In this section, we mainly study the influence of different Reynolds number on flow distribution. The established model is shown in Fig. 5 and 7(a). One inlet and five outlets are set. The velocity of inlet is $\nu = -1$. Assumed that the computational domain is horizontal, the influence of fluid gravity is not considered. The simulation results are shown in Fig. 7(b)-7(d).

Through the simulation, it is found that with the increase of Reynolds number, the flow rate of the outlet 3 increased significantly. When the Reynolds number reached 100, the vortex began to appear around outlets 1, 2, 4 and 5. As the Reynolds number increased to 1000, the vortex becomes larger and larger. When the Reynolds number is relatively small, there is little fluid outflow at outlets 1 and 5. With the increase of Reynolds number, the outlets 1 and 5 not only no outflow, but also have reflux phenomenon.

5. Conclusions

(1) In the direct water inrush, the Reynolds number has a significant effect on the distribution of water flow and vortex occurred when Reynolds numbers are large.

(2) With the increase of Reynolds numbers, the water flow of the wider fractures decreased gradually and the water flow of the Narrow fractures increased gradually. And finally the steady-state was reached.

(3) When the flow regime changes from laminar to turbulent flow, the larger the angle between the inlet and outlet is, the more obvious the outflow increases. However, when the flow state is turbulent, the flow is no longer significant with the increase of Reynolds numbers.

Acknowledgements

The work is supported by National Basic Research

Program of China (Grant No.2013CB036000), National Natural Science Foundation of China (Grant No. 51609129, 51479107), State Key Lab of Subtropical Building Science, South China University of Technology (2016ZB07), State Key Laboratory for GeoMechanics and Deep Underground Engineering, China University of Mining & Technology (Grant No. SKLGDUEK1515), Shandong Provincial Natural Science Foundation, China (Grant No. ZR2014EEQ002), China Postdoctoral Science Foundation (2017T100492, 2017M612273) and Shandong postdoctoral innovation project special Foundation (Grant No. 201502025). Prof. Shu-cai Li is the Corresponding author.

References

Barton, K.J. and Derham, J. (1987), “Geophysical surveys over fracture-zones in the galway granite at mace head, Co Galway, Ireland”, *Geophys. J. Royal Astron. Soc.*, **89**(1), 456-456.

He, Y., Tao, Y. and Yang, L. (2010), “Experimental research on hydraulic behaviors in a single joint with various values of JRC”, *Chin. J. Rock Mech. Eng.*, **29**(S1), 3235-3240.

Indraratna, B. and Ranjith, P.G. (2001), “Laboratory measurement of two-phase flow parameters in rock joints based on high pressure triaxial testing”, *J. Geotech. Geoenviron.*, **127**(6), 530-542.

Johnson, J., Brown, S. and Stockman, H. (2006), “Fluid flow and mixing in rough-walled fracture intersections”, *J. Geophys. Res. Solid Earth*, **111**(B12), 206.

Kosakowski, G. and Berkowitz, B. (1999), “Flow pattern variability in natural fracture intersections”, *Geophys. Res. Lett.*, **26**(12), 1765-1768.

Li, S.C., Wu, J., Xu, Z.H., Li, L.P., Huang, X., Xue, Y.G. and Wang, Z.C. (2016), “Numerical analysis of water flow characteristics after inrushing from the tunnel floor in process of karst tunnel excavation”, *Geomech. Eng.*, **10**(4), 471-526.

Mourzenko, V.V., Thovert, J.F. and Adler, P.M. (1995), “Permeability of a single fracture: Validity of the Reynolds equation”, *J. Phys. II*, **5**(3), 465-482.

Nelson, R. (2001), *Geologic Analysis of Naturally Fractured Reservoirs*, Gulf Professional Publishing, Woburn, Massachusetts, U.S.A.

Niroumand, H., Mehrizi, M.E.M. and Saaly, M. (2016), “Application of mesh-free smoothed particle hydrodynamics (SPH) for study of soil behavior”, *Geomech. Eng.*, **11**(1), 1-39.

Patera, A.T. (1984), “A spectral element method for fluid dynamics: Laminar flow in a channel expansion”, *J. Comput. Phys.*, **54**(3), 468-488.

Singhal, B.B.S. and Gupta, R.P. (2010), *Fractures and Discontinuities*, Springer, The Netherlands.

Singhal, B.B.S. and Gupta, RP. (2010), *Applied Hydrogeology of Fractured Rocks*, Springer, The Netherlands.

Sultan, M.A., Fonte, C.P., Dias, M.M., Lopes, J.C.B. and Santos, R.J. (2012), “Experimental study of flow regime and mixing in T-jets mixers”, *Chem. Eng. Sci.*, **73**, 388-399.

Tartakovsky, AM., Trask, N. and Pan, K. (2016), “Smoothed particle hydrodynamics and its applications for multiphase flow and reactive transport in porous media”, *Comput. Geosci.*, **20**(4), 807-834.

Wang, Z.L., Shen, L.F., Li, S.J and Xu, Z.M. (2017), “Seepage characteristics of a single fracture based on lattice Boltzmann method”, *Rock Soil Mech.*, **38**(4), 1203-1210.

Wang, Z.S., Li, Y., Zhu, W.S., Xue, Y.G., Jiang, B. and Sun, Y.B. (2017), “Field monitoring of splitting failure for surrounding rock masses and applications of energy dissipation model”, *Geomech. Eng.*, **12**(4), 595-609.

Wilson, C.R. and Witherspoon, P.A. (1976), “Flow interference effects at fracture intersections”, *Water Resour. Res.*, **12**(1), 102-104.

Zhou, Y. (2015), “Study on water inrush mechanism and early warning of filled piping-type disaster and its engineering applications in tunnels”, Ph.D. Dissertation, Shandong University, Jinan, China.

CC